Ain Shams Engineering Journal (2014) xxx, xxx–xxx

Ain Shams University

Ain Shams Engineering Journal

www.elsevier.com/locate/asej
www.sciencedirect.com

MECHANICAL ENGINEERING

Influence of heat transfer on MHD flow in a pipe with expanding or contracting permeable wall

S. Srinivas [a,*], A. Subramanyam Reddy [a], T.R. Ramamohan [b], Anant Kant Shukla [b]

[a] Fluid Dynamics Division, School of Advanced Sciences, VIT University, Vellore 632014, India
[b] CSIR-CMMACS, Wind Tunnel Road, Bangalore 560 037, India

Received 24 November 2013; revised 29 January 2014; accepted 30 January 2014

KEYWORDS

Porous pipe;
Permeation Reynolds number;
Wall expansion ratio;
Prandtl number;
Hartmann number;
HAM

Abstract The present study investigates the effects of heat transfer on MHD laminar viscous flow in a pipe with expanding or contracting permeable wall. The pipe wall expands or contracts uniformly at a time dependent rate. The governing equations are reduced to ordinary differential equations by using a similarity transformation. An analytical approach, namely the homotopy analysis method (HAM) is applied in order to obtain the solutions of the ordinary differential equations. The effects of various emerging parameters on flow variables have been discussed numerically and explained graphically. Further, we find a good agreement between the HAM solutions and solutions already reported in the literature.

© 2014 Production and hosting by Elsevier B.V. on behalf of Ain Shams University.

1. Introduction

A lot of attention has been given to the studies pertaining to laminar flow in a porous pipe or channel with expanding or contracting walls due to their wide applications in technological as well as biological flows, for example in the transport of biological fluids through expanding or contracting vessels, the synchronous pulsation of porous diaphragms, the air circulation in the respiratory system and the regression of the burning surface in solid rocket motors [1–7]. The viscous flow inside an impermeable tube of contracting cross section was first examined by Uchida and Aoki [8]. Therein, the Navier–Stokes equations for a semi-infinite tube were reduced to a single differential equation. They investigated a similar solution for the unsteady flows produced by a singe contraction or expansion of the wall of a semi-infinite circular pipe. Goto and Uchida [9] carried out a theoretical analysis of the unsteady flow in a semi-infinite expanding or contracting circular pipe into which an incompressible fluid is injected or sucked in through the wall surface. Bujurke et al. [10] have studied the unsteady flow in a contracting or expanding pipe by using a computer extended series solution. Boutros et al. [11] have applied the Lie-group method for unsteady flows in a semi-infinite expanding or contracting pipe with injection or suction through a porous wall. In their investigation the Lie-group method was applied to the equations of the motion for determining symmetry reductions in partial differential equations, the resulting fourth order differential equation was then solved using

* Corresponding author. Tel.: +91 416 2202514; fax: +91 416 2243092.
E-mail address: srinusuripeddi@hotmail.com (S. Srinivas).
Peer review under responsibility of Ain Shams University.

ELSEVIER Production and hosting by Elsevier

2090-4479 © 2014 Production and hosting by Elsevier B.V. on behalf of Ain Shams University.
http://dx.doi.org/10.1016/j.asej.2014.01.006

Please cite this article in press as: Srinivas S et al., Influence of heat transfer on MHD flow in a pipe with expanding or contracting permeable wall, Ain Shams Eng J (2014), http://dx.doi.org/10.1016/j.asej.2014.01.006

small-parameter perturbations and the results were compared with numerical solutions using a shooting method coupled with a Runge–Kutta scheme. Xinhui et al. [12] have analyzed the problem of laminar flow in a porous pipe with suction at slowly expanding or contracting wall. Majdalani and Zhou [13] studied moderate to large injection and suction driven channel flows with expanding or contracting walls. In this investigation the governing equation is first integrated and the resulting third-order differential equation is solved using the method of variation in parameters, for the large injection case. For the large suction case, the governing equation is first simplified near the wall and then solved using successive approximations.

There has been growing interest in studying the magnetohydrodynamic (MHD) flow and heat transfer characteristics of electrically conducting fluids because of many practical applications such as in MHD flowmetry, MHD power generation MHD pumps, high temperature plasmas, chemical processing equipment, power generation systems and cooling of nuclear reactors [14–18]. Hayat et al. [19] have obtained explicit analytical solutions for MHD pipe flow of a fourth grade fluid. Xinhui et al. [20] discussed the unsteady flow in a porous channel with expanding or contracting walls in the presence of a transverse magnetic field using the singular perturbation method. Turkyilmazoglu [21] obtained exact solutions for the steady Navier–Stokes equations governing the incompressible viscous Newtonian electrically conducting fluid flow due to rotating disk. Makinde et al. [22] have examined wall driven steady flow of a viscous fluid and heat transfer in a uniformly porous tube using perturbation series. Nakhi and Chamkha [23] analyzed the conjugate natural convection around a finned pipe in a square enclosure with internal heat generation. Recently, Srinivas et al. ([24] several references therein) studied the thermal diffusion and diffusion thermo effects in a two-dimensional viscous flow between slowly expanding or contracting walls with weak permeability. Reddy et al. [25] analyzed the influence of heat transfer and chemical reaction on asymmetric laminar flow between two slowly expanding or contracting walls using a double perturbation in the permeation Reynolds number and the wall expansion ratio. More recently, Srinivas et al. [26] have examined the effects of mass transfer and chemical reaction on laminar flow in a porous pipe with expanding or contracting wall by using the homotopy analysis method.

A literature survey reveals that no attempt regarding heat transfer effects on MHD flow of viscous fluid in a porous pipe with expanding or contracting wall has been made so far. Such a study is of great value in biological and engineering research. Hence the main aim of this work is to study the effect of heat transfer on MHD viscous flow in a porous pipe with expanding or contracting wall. The governing equations in cylindrical coordinates are introduced and transformed into ordinary differential equations using similarity transformations and then solved using a powerful technique recently developed by Liao [27] namely the homotopy analysis method (HAM). This technique has been applied successfully to many interesting problems ([28-35]). The features of the flow characteristics are analyzed by plotting graphs and are discussed in detail. The present paper is organized in the following manner. In Section 2, details of the mathematical formulation are presented. Sections 2.1 and 2.2 include the solution procedure of the problem. Numerical results and discussion are given in Section 3 and the conclusions have been summarized in Section 4.

2. Formulation of the problem

Consider the laminar and incompressible electrically conducting fluid flow in a porous pipe of a semi-infinite length with an expanding or contracting wall. The radius of the pipe is $a(t)$. The wall has equal permeability and expands or contracts uniformly at a time dependent rate $\dot{a}(t)$. A magnetic field of uniform strength B_0 is applied perpendicular to the wall. A coordinate system can be chosen with the origin at the center of the pipe as shown in Fig. 1. Take the $\hat{z}$ coordinate axis parallel to the pipe wall and the $\hat{r}$ coordinate axis perpendicular to the wall. Under these assumptions the governing equations are ([8], [11], and [12])

$$\frac{\partial \hat{u}}{\partial \hat{z}} + \frac{\partial \hat{v}}{\partial \hat{r}} + \frac{\hat{v}}{\hat{r}} = 0, \tag{1}$$

$$\frac{\partial \hat{u}}{\partial t} + \hat{u}\frac{\partial \hat{u}}{\partial \hat{z}} + \hat{v}\frac{\partial \hat{u}}{\partial \hat{r}} = -\frac{1}{\rho}\frac{\partial \hat{p}}{\partial \hat{z}} + \nu\left(\frac{\partial^2 \hat{u}}{\partial \hat{z}^2} + \frac{\partial^2 \hat{u}}{\partial \hat{r}^2} + \frac{1}{\hat{r}}\frac{\partial \hat{u}}{\partial \hat{r}}\right) - \frac{\sigma B_0^2}{\rho}\hat{u}, \tag{2}$$

$$\frac{\partial \hat{v}}{\partial t} + \hat{u}\frac{\partial \hat{v}}{\partial \hat{z}} + \hat{v}\frac{\partial \hat{v}}{\partial \hat{r}} = -\frac{1}{\rho}\frac{\partial \hat{p}}{\partial \hat{r}} + \nu\left(\frac{\partial^2 \hat{v}}{\partial \hat{z}^2} + \frac{\partial^2 \hat{v}}{\partial \hat{r}^2} + \frac{1}{\hat{r}}\frac{\partial \hat{v}}{\partial \hat{r}} - \frac{\hat{v}}{\hat{r}^2}\right), \tag{3}$$

$$\frac{\partial T}{\partial t} + \hat{u}\frac{\partial T}{\partial \hat{z}} + \hat{v}\frac{\partial T}{\partial \hat{r}} = \frac{\kappa}{\rho c_p}\left(\frac{\partial^2 T}{\partial \hat{z}^2} + \frac{\partial^2 T}{\partial \hat{r}^2} + \frac{1}{\hat{r}}\frac{\partial T}{\partial \hat{r}}\right) \tag{4}$$

where $\hat{u}, \hat{v}$ are the components of velocity along the $\hat{z}$ and $\hat{r}$ directions respectively, ρ is density, $\hat{p}$ is dimensional pressure, t is time, ν is kinematic viscosity, σ is electrical conductivity, B_0 is the strength of applied magnetic field, c_p is specific heat at constant pressure, κ is thermal conductivity, and T is the temperature of the fluid.

The boundary conditions are as follows:

$$\hat{u} = 0, \quad \hat{v} = -v_w = -A\dot{a}, \quad T = T_w \quad \text{at } \hat{r} = a(t) \tag{5}$$

$$\frac{\partial \hat{u}}{\partial \hat{r}} = 0, \hat{v} = 0, \quad \frac{\partial T}{\partial \hat{r}} = 0 \quad \text{at } \hat{r} = 0 \tag{6}$$

$$\hat{u} = 0, \hat{v} = 0 \quad \text{at } \hat{z} = 0 \tag{7}$$

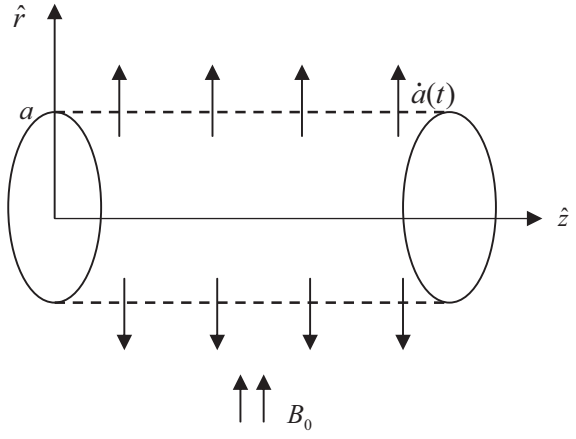

Figure 1 Porous pipe with expanding or contracting wall.

Please cite this article in press as: Srinivas S et al., Influence of heat transfer on MHD flow in a pipe with expanding or contracting permeable wall, Ain Shams Eng J (2014), http://dx.doi.org/10.1016/j.asej.2014.01.006

The injection/suction coefficient A that appears in Eq. (5) is the measure of wall permeability. Introduce a stream function which satisfies the continuity Eq. (1)

$$\widehat{\psi} = v\hat{z}\widehat{F}(\eta, t) \tag{8}$$

where $\boldsymbol{\eta} = \frac{\hat{r}}{a}$ is the dimensionless radial position.

The axial and radial velocity components can be written as

$$\hat{u} = \frac{1}{\hat{r}}\frac{\partial\widehat{\psi}}{\partial\hat{r}} = \frac{v\hat{z}\widehat{F}_{\boldsymbol{\eta}}(\boldsymbol{\eta}, t)}{a^2\boldsymbol{\eta}} \quad \text{and} \quad \hat{v} = -\frac{1}{\hat{r}}\frac{\partial\widehat{\psi}}{\partial\hat{z}} = -\frac{v\widehat{F}(\boldsymbol{\eta}, t)}{a\boldsymbol{\eta}} \tag{9}$$

Substituting Eq. (9) into Eqs. (2) and (3) and then eliminating pressure, one obtains

$$\begin{aligned}\boldsymbol{\eta}^2\widehat{F}_{\boldsymbol{\eta}\boldsymbol{\eta}\boldsymbol{\eta}\boldsymbol{\eta}\boldsymbol{\eta}} + (\boldsymbol{\alpha}\boldsymbol{\eta}^3 - 2\boldsymbol{\eta})\widehat{F}_{\boldsymbol{\eta}\boldsymbol{\eta}\boldsymbol{\eta}} + (\boldsymbol{\eta}^2\boldsymbol{\alpha} + 3)\widehat{F}_{\boldsymbol{\eta}\boldsymbol{\eta}} - \left(\boldsymbol{\eta}\boldsymbol{\alpha} + \frac{3}{\boldsymbol{\eta}}\right)\widehat{F}_{\boldsymbol{\eta}} \\ + \widehat{F}_{\boldsymbol{\eta}}^2 - \boldsymbol{\eta}\widehat{F}_{\boldsymbol{\eta}}\widehat{F}_{\boldsymbol{\eta}\boldsymbol{\eta}} + \boldsymbol{\eta}\widehat{F}\widehat{F}_{\boldsymbol{\eta}\boldsymbol{\eta}\boldsymbol{\eta}} - 3\widehat{F}\widehat{F}_{\boldsymbol{\eta}\boldsymbol{\eta}} \\ + \frac{3}{\boldsymbol{\eta}}\widehat{F}\widehat{F}_{\boldsymbol{\eta}} - M^2(\boldsymbol{\eta}^2\widehat{F}_{\boldsymbol{\eta}\boldsymbol{\eta}} - \boldsymbol{\eta}\widehat{F}_{\boldsymbol{\eta}}) - \frac{a^2}{\boldsymbol{\nu}}\boldsymbol{\eta}^3\left(\frac{\widehat{F}_{\boldsymbol{\eta}}}{\boldsymbol{\eta}}\right)_{\boldsymbol{\eta}t} = 0\end{aligned} \tag{10}$$

where $\alpha(t) = a\dot{a}/v$ is the non-dimensional wall dilation rate and is defined to be positive for expansion and negative for contraction and $M = \frac{\sqrt{\sigma}B_0 a}{\sqrt{\mu}}$ is the Hartmann number and $\boldsymbol{\mu}$ is dynamic viscosity. The boundary conditions given by Eqs. (5) and (6) translate into

$$\begin{aligned}&\widehat{F}(0,t) = 0, \widehat{F}(1,t) = R, \widehat{F}_{\boldsymbol{\eta}}(1,t) \\ &= 0, \lim_{\boldsymbol{\eta}\to 0}\frac{\partial}{\partial\boldsymbol{\eta}}\left(\frac{1}{\boldsymbol{\eta}}\frac{\partial\widehat{F}(\boldsymbol{\eta}, t)}{\partial\boldsymbol{\eta}}\right) = 0\end{aligned} \tag{11}$$

where R is the permeation Reynolds number and is defined by $R = av_w/\boldsymbol{\nu} = A\boldsymbol{\alpha}$. Note that R is positive for injection and negative for suction. A similar solution with respect to both space and time can now be developed by following the transformation described by Uchida and Aoki [8] and Majdalani and Zhou [13] independently. For constant $\boldsymbol{\alpha}$ and $\widehat{F} = \widehat{F}(\boldsymbol{\eta})$, it follows that $\left(\frac{\widehat{F}_{\boldsymbol{\eta}}}{\boldsymbol{\eta}}\right)_{\boldsymbol{\eta}t} = 0$. To realize this condition, the value of the expansion ratio $\boldsymbol{\alpha}$ must be specified by the initial value

$$\boldsymbol{\alpha} = \frac{a\dot{a}}{\boldsymbol{\nu}} = \frac{a_0\dot{a}_0}{\boldsymbol{\nu}} = \text{constant}, \quad \text{or } \frac{\dot{a}_0}{\dot{a}} = \frac{a}{a_0}, \tag{12}$$

where a_0 and $\dot{a}_0$ denote the initial height and expansion rate. Forthwith, the temporal similarity transformation can be achieved by integrating Eq. (12) with respect time. The result is

$$\frac{a}{a_0} = \sqrt{1 + 2\boldsymbol{\nu}\boldsymbol{\alpha}ta_0^{-2}}. \tag{13}$$

Since $v_w = A\dot{a}$, an expression for the injection velocity can be determined, proved that the injection coefficient A is constant. From Eqs. (12) and (13), it is clear that

$$\frac{\dot{a}_0}{\dot{a}} = \frac{v_w(0)}{v_w(t)} = \sqrt{1 + 2\boldsymbol{\nu}\boldsymbol{\alpha}ta_0^{-2}}.$$

Under these provisions (10) becomes,

$$\begin{aligned}&\boldsymbol{\eta}^3\widehat{F}^{IV} + \boldsymbol{\alpha}(\boldsymbol{\eta}^4\widehat{F}''' + \boldsymbol{\eta}^3\widehat{F}'' - \boldsymbol{\eta}^2\widehat{F}') - 2\boldsymbol{\eta}^2\widehat{F}''' + 3\boldsymbol{\eta}\widehat{F}'' \\ &- 3\widehat{F}' + \boldsymbol{\eta}\widehat{F}^2 - \boldsymbol{\eta}^2\widehat{F}'\widehat{F}'' - 3\boldsymbol{\eta}\widehat{F}\widehat{F}'' + 3\widehat{F}\widehat{F}' + \boldsymbol{\eta}^2\widehat{F}\widehat{F}''' \\ &- M^2(\boldsymbol{\eta}^3\widehat{F}'' - \boldsymbol{\eta}^2\widehat{F}') \\ &= 0\end{aligned} \tag{14}$$

The corresponding boundary conditions are

$$\widehat{F}(0) = 0, \quad \widehat{F}(1) = R, \quad \widehat{F}'(1) = 0, \quad \lim_{\boldsymbol{\eta}\to 0}\left(\frac{\widehat{F}'}{\boldsymbol{\eta}}\right)' = 0 \tag{15}$$

Eqs. (9), (14), and (15) can be normalized by putting

$$\boldsymbol{\psi} = \frac{\widehat{\psi}}{a\dot{a}}, \quad u = \frac{\hat{u}}{\dot{a}}, \quad v = \frac{\hat{v}}{\dot{a}}, \quad z = \frac{\hat{z}}{a}, \quad f = \frac{\widehat{F}}{R} \tag{16}$$

and so$u = \frac{zAf'}{\boldsymbol{\eta}}, v = -\frac{Af}{\boldsymbol{\eta}}$

$$\begin{aligned}&\boldsymbol{\eta}^3 f^{IV} + \boldsymbol{\alpha}(\boldsymbol{\eta}^4 f''' + \boldsymbol{\eta}^3 f'' - \boldsymbol{\eta}^2 f') - 2\boldsymbol{\eta}^2 f''' + 3\boldsymbol{\eta} f'' - 3f' \\ &+ \boldsymbol{\eta}Rf'^2 - \boldsymbol{\eta}^2 Rf'f'' - 3\boldsymbol{\eta}Rff'' + 3Rff' \\ &+ \boldsymbol{\eta}^2 Rff''' - M^2(\boldsymbol{\eta}^3 f'' - \boldsymbol{\eta}^2 f') = 0\end{aligned} \tag{17}$$

$$f(0) = 0, \quad f(1) = 1, \quad f'(1) = 0, \quad \lim_{\boldsymbol{\eta}\to 0}\left(\frac{f'}{\boldsymbol{\eta}}\right)' = 0 \tag{18}$$

When $\boldsymbol{\alpha} = 0$ and $M = 0$, Eq. (17) is the case that Majdalani and Flandro [7] have described.

The temperature of the fluid in the pipe can be expressed as [22]

$$T = T_0 + B\frac{\hat{z}}{a}\theta(\boldsymbol{\eta}) \tag{19}$$

where T_0 is the reference temperature at the center, B is constant of the fluid.

The dimensionless form of temperature from Eq. (19) is

$$\boldsymbol{\theta} = \frac{T - T_0}{T_w - T_0} \tag{20}$$

where T_w is the temperature at the wall.

Substituting Eq. (19) into Eq. (4), one obtains

$$\boldsymbol{\eta}\boldsymbol{\theta}'' + \boldsymbol{\alpha}\text{Pr}(\boldsymbol{\eta}^2\boldsymbol{\theta}' + \boldsymbol{\eta}\boldsymbol{\theta}) - R\text{Pr}f'\boldsymbol{\theta} + R\text{Pr}f\boldsymbol{\theta}' + \boldsymbol{\theta}' = 0 \tag{21}$$

where $\text{Pr} = \frac{\mu c_p}{\kappa}$ is Prandtl number. The corresponding boundary conditions are

$$\boldsymbol{\theta}'(0) = 0, \boldsymbol{\theta}(1) = 1 \tag{22}$$

2.1. Solution of the problem

To develop analytical solutions by HAM as a polynomial base function, the boundary conditions in Eq. (18) become:

$$f(0) = 0, \quad f(1) = 1, \quad f'(1) = 0, \quad f'(0) = 0 \tag{23}$$

For the HAM solution of Eqs. (17) and (21), the initial approximations f_0 and $\boldsymbol{\theta}_0$ and auxiliary linear operators L_1 and L_2 are

$$f_0(\boldsymbol{\eta}) = 3\boldsymbol{\eta}^2 - 2\boldsymbol{\eta}^3 \tag{24}$$

$$\boldsymbol{\theta}_0(\boldsymbol{\eta}) = 1 \tag{25}$$

$$L_1(f) = \frac{d^4 f}{d\boldsymbol{\eta}^4}; \quad L_2(\boldsymbol{\theta}) = \frac{d^2 f}{d\boldsymbol{\eta}^2} \tag{(26)-27}$$

$$\text{where} \quad L_1(c_1\boldsymbol{\eta}^3 + c_2\boldsymbol{\eta}^2 + c_3\boldsymbol{\eta} + c_4) = 0 \tag{28}$$

$$L_2(c_5\boldsymbol{\eta} + c_6) = 0 \tag{29}$$

Please cite this article in press as: Srinivas S et al., Influence of heat transfer on MHD flow in a pipe with expanding or contracting permeable wall, Ain Shams Eng J (2014), http://dx.doi.org/10.1016/j.asej.2014.01.006

and $c_i (i = 1-6)$ are constants.

2.1.1. Zero-order deformation equations

Let $p \in [0, 1]$ be an embedding parameter and h be the auxiliary non-zero parameter. The deformation equations at zero-order can be written as follows

$$(1-p)L_1[\widehat{f}(\eta;p) - f_0(\eta)] = phN_1[\widehat{f}(\eta;p)] \tag{30}$$

$$\widehat{f}(0;p) = 0, \widehat{f}(1;p) = 1, \widehat{f}'(1;p) = 0, \widehat{f}'(0;p) = 0, \tag{31}$$

$$(1-p)L_2[\widehat{\theta}(\eta;p) - \theta_0(\eta)] = phN_2[\widehat{\theta}(\eta;p), \widehat{f}(\eta;p)] \tag{32}$$

$$\widehat{\theta}(1;p) = 1, \widehat{\theta}\,'(0;p) = 0 \tag{33}$$

where

$$\begin{aligned} N_1[\widehat{f}(\eta;p)] &= \eta^3 \frac{\partial^4 \widehat{f}(\eta;p)}{\partial \eta^4} \\ &+ \alpha\left[\eta^4 \frac{\partial^3 \widehat{f}(\eta;p)}{\partial \eta^3} + \eta^3 \frac{\partial^2 \widehat{f}(\eta;p)}{\partial \eta^2} - \eta^2 \frac{\partial \widehat{f}(\eta;p)}{\partial \eta}\right] \\ &- 2\eta^2 \frac{\partial^3 \widehat{f}(\eta;p)}{\partial \eta^3} + 3\eta \frac{\partial^2 \widehat{f}(\eta;p)}{\partial \eta^2} - 3\frac{\partial \widehat{f}(\eta;p)}{\partial \eta} \\ &+ R\eta\left[\frac{\partial \widehat{f}(\eta;p)}{\partial \eta}\right]^2 - R\eta^2 \frac{\partial \widehat{f}(\eta;q)}{\partial \eta}\frac{\partial^2 \widehat{f}(\eta;p)}{\partial \eta^2} \\ &- 3R\eta \widehat{f}(\eta;p)\frac{\partial^2 \widehat{f}(\eta;p)}{\partial \eta^2} + 3R\eta \widehat{f}(\eta;q) \\ &\times \frac{\partial \widehat{f}(\eta;p)}{\partial \eta} + R\eta^2 \widehat{f}(\eta;q)\frac{\partial^3 \widehat{f}(\eta;p)}{\partial \eta^3} \\ &- M^2\left[\eta^3 \frac{\partial^2 \widehat{f}(\eta;p)}{\partial \eta^2} - \eta^2 \frac{\partial \widehat{f}(\eta;p)}{\partial \eta}\right] \end{aligned} \tag{34}$$

$$\begin{aligned} N_2[\widehat{\theta}(\eta;p), \widehat{f}(\eta;p)] &= \eta \frac{\partial^2 \widehat{\theta}(\eta;p)}{\partial \eta^2} \\ &+ \alpha \mathrm{Pr}\left[\eta^2 \frac{\partial \widehat{\theta}(\eta;p)}{\partial \eta} + \eta \widehat{\theta}(\eta;p)\right] \\ &- R\mathrm{Pr}\frac{\partial \widehat{f}(\eta;p)}{\partial \eta}\widehat{\theta}(\eta;p) + R\mathrm{Pr}\widehat{f}(\eta;p) \\ &\times \frac{\partial \widehat{\theta}(\eta;p)}{\partial \eta} + \frac{\partial \widehat{\theta}(\eta;p)}{\partial \eta} \end{aligned} \tag{35}$$

For $p = 0$ and $p = 1$, we have

$$\widehat{f}(\eta;0) = f_0(\eta), \quad \widehat{f}(\eta;1) = f(\eta) \tag{36}$$

$$\widehat{\theta}(\eta;0) = \theta_0(\eta), \quad \widehat{\theta}(\eta;1) = \theta(\eta) \tag{37}$$

Further by Taylor's series expansion one obtains

$$\begin{aligned} f(\eta) &= f_0(\eta) + \sum_{m=1}^{\infty} f_m(\eta)p^m \quad \text{where } f_m(\eta) \\ &= \frac{1}{m!}\frac{\partial^m \widehat{f}(\eta;p)}{\partial p^m}\bigg|_{p=0} \end{aligned} \tag{38}$$

and

$$\begin{aligned} \theta(\eta) &= \theta_0(\eta) + \sum_{m=1}^{\infty} \theta_m(\eta)p^m \quad \text{where } \theta_m(\eta) \\ &= \frac{1}{m!}\frac{\partial^m \widehat{\theta}(\eta;p)}{\partial p^m}\bigg|_{p=0} \end{aligned} \tag{39}$$

We choose proper h in such a way that these series are convergent at $p = 1$, therefore we have the solution expressions from Eqs. (38) and (39) as follows:

$$f(\eta) = f_0(\eta) + \sum_{m=1}^{\infty} f_m(\eta) \tag{40}$$

$$\theta(\eta) = \theta_0(\eta) + \sum_{m=1}^{\infty} \theta_m(\eta) \tag{41}$$

2.1.2. The high-order deformation equations

Differentiating the zero-order deformation Eqs. (30) and (32) m times with respect to p, then dividing by $m!$, and finally setting $p = 0$, one obtains the following m th order deformation equations:

$$L_1[f_m(\eta) - \chi_m f_{m-1}(\eta)] = hR_{1,m}(\eta) \tag{42}$$

$$L_2[\theta_m(\eta) - \chi_m \theta_{m-1}(\eta)] = hR_{2,m}(\eta) \tag{43}$$

together with the conditions

$$f_m(0) = f_m(1) = f'_m(1) = f'_m(0) = 0 \tag{44}$$

$$\theta_m(1) = \theta'_m(0) = 0 \tag{45}$$

$$\chi_m = \begin{vmatrix} 1, & m \neq 1 \\ 0, & m = 1 \end{vmatrix} \tag{46}$$

where

$$\begin{aligned} R_{1,m} &= \eta f^{IV}_{m-1} + \alpha[\eta^4 f''_{m-1} + \eta^3 f''_{m-1} - \eta^2 f'_{m-1}] - 2\eta^2 f'''_{m-1} \\ &+ 3\eta f''_{m-1} - 3f'_{m-1} + R\eta\sum_{k=0}^{m-1} f'_{m-1-k}f'_k \\ &- R\eta^2\sum_{k=0}^{m-1} f'_{m-1-k}f''_k - 3R\eta\sum_{k=0}^{m-1} f_{m-1-k}f''_k + 3R\sum_{k=0}^{m-1} f_{m-1-k}f'_k \\ &+ R\eta^2\sum_{k=0}^{m-1} f_{m-1-k}f'''_k - M^2[\eta^3 f''_{m-1} - \eta^2 f'_{m-1}] \end{aligned} \tag{47}$$

$$\begin{aligned} R_{2,m} &= \eta\theta''_{m-1} + \alpha\mathrm{Pr}[\eta^2\theta'_{m-1} + \eta\theta_{m-1}] - R\mathrm{Pr}\sum_{k=0}^{m-1} f'_{m-1-k}\theta_k \\ &+ R\mathrm{Pr}\sum_{k=0}^{m-1} f_{m-1-k}\theta'_k + \theta'_{m-1} \end{aligned} \tag{48}$$

For each m, to solve Eqs. (42) and (43) with the conditions (44) and (45) we follow [27–33].

2.2. Convergence of HAM solution

As pointed out by Liao [27], the convergence of the series depends upon h which determines the convergence region for HAM. If h is properly chosen, the homotopy series solution may converge fast. For this purpose h-curves are plotted in Fig. 2 for the 20th order approximation. From Fig. 2, the re-

gion of convergence for admissible values of h is $-1.1 \leqslant h \leqslant -0.2$.

One can define the square residual error to prove the correctness of the h-curves. Substituting the approximate solutions of $f(\boldsymbol{\eta})$ and $\boldsymbol{\theta}(\boldsymbol{\eta})$ obtained by the HAM into Eqs. (17) and (21) yields the residual error as follows:

$$\begin{aligned} E_1 &= \boldsymbol{\eta}^3 f^{IV} + \boldsymbol{\alpha}(\boldsymbol{\eta}^4 f''' + \boldsymbol{\eta}^3 f'' - \boldsymbol{\eta}^2 f') - 2\boldsymbol{\eta}^2 f''' + 3\boldsymbol{\eta} f'' \\ &\quad - 3f' + \boldsymbol{\eta} R f'^2 - \boldsymbol{\eta}^2 R f' f'' - 3\boldsymbol{\eta} R f f'' + 3R f f' \\ &\quad + \boldsymbol{\eta}^2 R f f''' - M^2(\boldsymbol{\eta}^3 f'' - \boldsymbol{\eta}^2 f') \\ &= 0 \end{aligned} \tag{49}$$

$$E_2 = \boldsymbol{\eta}\theta'' + \boldsymbol{\alpha}\mathrm{Pr}(\boldsymbol{\eta}^2\boldsymbol{\theta}' + \boldsymbol{\eta}\boldsymbol{\theta}) - R\mathrm{Pr} f'\boldsymbol{\theta} + R\mathrm{Pr} f\boldsymbol{\theta}' + \boldsymbol{\theta}' \tag{50}$$

where E_1 and E_2 correspond to the residual error for $f(\boldsymbol{\eta})$ and $\boldsymbol{\theta}(\boldsymbol{\eta})$respectively. We show the square residual error (SRE) for $f(\boldsymbol{\eta})$ and $\boldsymbol{\theta}(\boldsymbol{\eta})$obtained by different approximations in Tables 1a and 1b. From this table it can be seen that the different values of h lead to minimum average square residual error for $f(\boldsymbol{\eta})$ and $\boldsymbol{\theta}(\boldsymbol{\eta})$. It is clear that the average square residual error decreases monotonically as the order of approximation increases. Further, the shear stress can be obtained from Newton's law of viscosity

$$\hat{\boldsymbol{\tau}} = \boldsymbol{\mu}\left[\frac{\partial \hat{v}}{\partial \hat{z}} + \frac{\partial \hat{u}}{\partial \hat{r}}\right] = \boldsymbol{\mu}\frac{\partial \hat{u}}{\partial \hat{r}} \tag{51}$$

Introducing dimensionless shear stress $\boldsymbol{\tau} = \frac{\hat{\boldsymbol{\tau}}}{\rho v_w^2}$, Eq. (51) becomes

$$\boldsymbol{\tau} = zR^{-1}\left(\frac{1}{\boldsymbol{\eta}}f'' - \frac{1}{\boldsymbol{\eta}^2}f'\right) \tag{52}$$

At the pipe wall the dimensionless shear stress is [8]

$$\boldsymbol{\tau} = zR^{-1}f''(1) \tag{53}$$

To obtain the radial pressure drop, substituting the velocity components into Eq. (3), one obtains

$$P_\eta = \left(-R^{-1}\boldsymbol{\alpha} f - \frac{1}{2}\left(\frac{f^2}{\boldsymbol{\eta}^2}\right) - R^{-1}\left(\frac{f'}{\boldsymbol{\eta}}\right)\right)' \tag{54}$$

The radial pressure distribution can now be determined by integrating Eq. (54). Letting P_c be the centerline pressure, one may proceed from

$$\int_{P_c}^{P(\boldsymbol{\eta})} dP = -\int_0^{\boldsymbol{\eta}} \left[R^{-1}\boldsymbol{\alpha} f + \frac{1}{2}\left(\frac{f^2}{\boldsymbol{\eta}^2}\right) + R^{-1}\left(\frac{f'}{\boldsymbol{\eta}}\right)\right]' d\boldsymbol{\eta} \tag{55}$$

The resulting radial pressure distribution will be [8]

$$\begin{aligned} \Delta P_r &\equiv P(\boldsymbol{\eta}) - P_c \\ &= R^{-1}\left[\frac{f'}{\boldsymbol{\eta}}\right]_{\boldsymbol{\eta}=0} - \left(\boldsymbol{\alpha}R^{-1}f + \frac{1}{2}\frac{f^2}{\boldsymbol{\eta}^2} + R^{-1}\left(\frac{f'}{\boldsymbol{\eta}}\right)\right) \end{aligned} \tag{56}$$

The heat transfer rate in terms of Nusselt number is defined as

$$Nu = \frac{h_m a}{\boldsymbol{\kappa}} \tag{57}$$

where h_m is the heat transfer coefficient defined as

$$h_m(T_w - T_0) = -\boldsymbol{\kappa}\frac{dT}{d\hat{r}} \tag{58}$$

Hence the dimensionless Nusselt number at the pipe wall is defined as

$$Nu = -\boldsymbol{\theta}'(1) \tag{59}$$

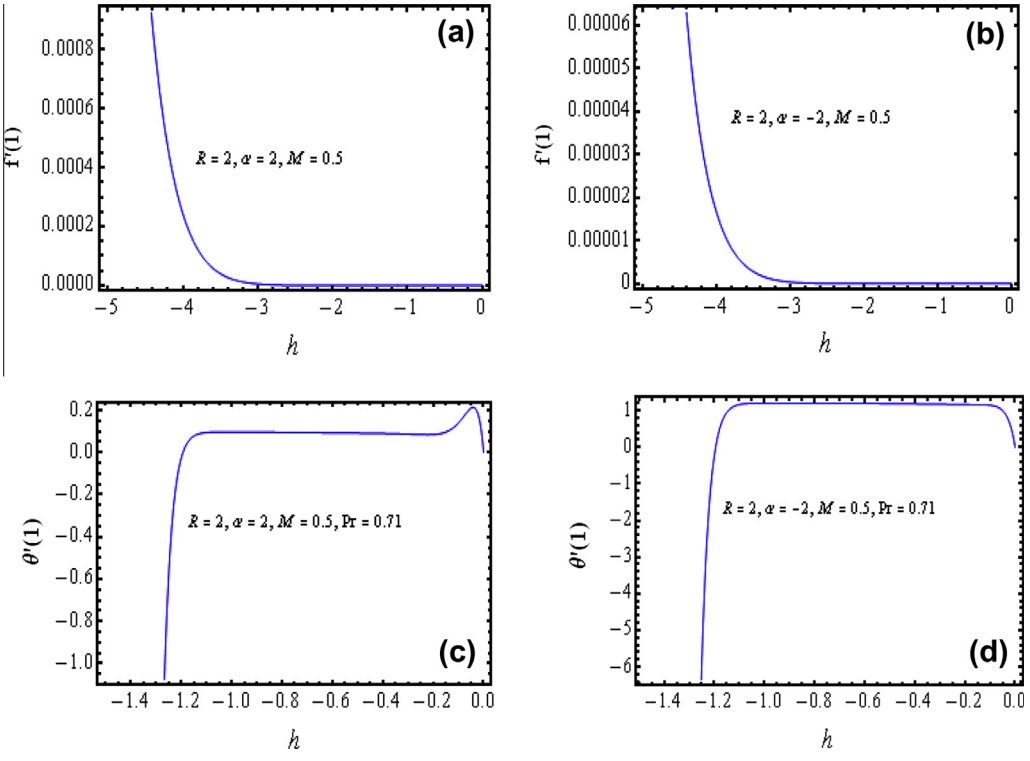

Figure 2 h Curves for the 20th order approximations for the functions f, $\boldsymbol{\theta}$.

Table 1a 15th and 20th order approximations for the optimal convergence-control parameter h and corresponding average square residual error (SRE) in the case of $R = 2$, $\alpha = 1$, $M = 0.5$ for the solution of f and $R = 2$, $\alpha = 1$, Pr = 0.71, $M = 0.5$ for the solution of $\boldsymbol{\theta}$.

Convergence Control parameter (h)	SRE of f		SRE of $\boldsymbol{\theta}$	
	15th order	20th order	15th order	20th order
−0.6	2.59856×10^{-1}	1.27499×10^{-1}	6.82445×10^{-4}	3.0693×10^{-4}
−0.7	1.74033×10^{-1}	8.48657×10^{-2}	4.41923×10^{-4}	1.9797×10^{-4}
−0.8	1.22491×10^{-1}	5.9593×10^{-2}	3.02535×10^{-4}	1.35094×10^{-4}
−0.85	1.04359×10^{-1}	5.07573×10^{-2}	2.54548×10^{-4}	1.13496×10^{-4}
−0.9	8.97064×10^{-2}	4.36352×10^{-2}	2.16201×10^{-4}	9.62649×10^{-5}
−0.95	7.77335×10^{-2}	3.78265×10^{-2}	1.85051×10^{-4}	8.2355×10^{-5}
−1	6.78515×10^{-2}	3.30383×10^{-2}	1.6157×10^{-4}	7.11092×10^{-5}
−1.05	5.96203×10^{-2}	2.90531×10^{-2}	2.74247×10^{-4}	6.60378×10^{-5}

Table 1b 15th and 20th order approximations for the optimal convergence-control parameter h and corresponding average square residual error (SRE) in the case of $R = 2$, $\alpha = -1$, $M = 0.5$ for the solution of f and $R = 2$, $\alpha = -1$, Pr = 0.71, $M = 0.5$ for the solution of $\boldsymbol{\theta}$.

Convergence control parameter (h)	SRE of f		SRE of $\boldsymbol{\theta}$	
	15th order	20th order	15th order	20th order
−0.6	6.47564×10^{-1}	2.25058×10^{-1}	4.12343×10^{-4}	1.86556×10^{-4}
−0.7	3.51498×10^{-1}	1.22582×10^{-1}	2.67269×10^{-4}	1.20351×10^{-4}
−0.8	2.06482×10^{-1}	7.32308×10^{-2}	1.82983×10^{-4}	8.22146×10^{-5}
−0.85	1.62404×10^{-1}	5.82367×10^{-2}	1.53973×10^{-4}	6.91258×10^{-5}
−0.9	1.29713×10^{-1}	4.70693×10^{-2}	1.30667×10^{-4}	5.86886×10^{-5}
−0.95	1.05068×10^{-1}	3.8596×10^{-2}	1.110875×10^{-4}	5.03123×10^{-5}
−1	8.6205×10^{-2}	3.20578×10^{-2}	1.08353×10^{-4}	4.4445×10^{-5}
−1.05	7.1561×10^{-2}	2.6935×10^{-2}	8.43809×10^{-4}	8.21756×10^{-5}

3. Results and discussion

In order to get physical insight into the problem, dimensionless velocity components, temperature, shear stress, radial pressure drop and Nusselt number distributions have been discussed by assigning numerical values to various parameters that have been emerged in the mathematical formulation and the results are shown graphically in Figs. 3–17 for the proper value of $h = -1$. In order to illustrate the influence of permeation Reynolds number R, wall expansion ratio $\boldsymbol{\alpha}$, and Hartmann number M on the dimensionless axial velocity Figs. 3–5 are plotted. From these figures one can observe that the dimensionless axial velocity always reaches a maximum at the center. Fig. 3a and b shows the behavior of dimensionless axial velocity u/Az for $\boldsymbol{\alpha} = 2$ and $\boldsymbol{\alpha} = -2$ respectively, over a range of permeation Reynolds number R. For a constant wall expansion ratio $\boldsymbol{\alpha}$, the dimensionless axial velocity near the center increases with increasing suction (i.e. increasing $|R|$) while it decreases with increasing injection. More over the dimensionless axial velocity near the center for the case of suction combined with wall expansion is higher than the case of suction combined with wall contraction. Similar conclusions can be drawn by a comparison of the cases of injection combined with wall expansion and wall contraction. The dimensionless axial velocity for permeation Reynolds number $R = 2$ and $R = -1$ respectively, over a range of wall expansion ratio $\boldsymbol{\alpha}$ is plotted in Fig. 4a and b. For every level of suction or injection, for the case of wall expansion ($\boldsymbol{\alpha} > 0$), increasing $\boldsymbol{\alpha}$ leads to higher axial velocity near the center and lower near the wall. This is because when the wall is in expansion, the flow toward the center becomes greater to make up for the space caused by the expansion of the wall and as a result the axial velocity also becomes greater near the center. The behavior is reversed for the case of wall contraction ($\boldsymbol{\alpha} < 0$). In the limit of low expansion ratio, the dimensionless axial velocity distribution tends to parabolic for both $\boldsymbol{\alpha} > 0$ and $\boldsymbol{\alpha} < 0$. These observations are qualitatively in agreement with results of Majdalani et al. [1] and Srinivas et al. [24] for the case of hydrodynamic viscous flow in porous channel with expanding or contracting walls and with that of Uchida and Aoki [8] for the case of hydrodynamic viscous flow in a pipe with expanding or contracting wall. Fig. 5a–d depict the effect of Hartmann number on the dimensionless axial velocity. For a given increase in magnetic field strength, the dimensionless axial velocity decreases a little away the pipe wall. This is reasonable because we can assume that the magnetic force acts as a resistive drag force. The velocity is zero at the pipe wall and increases to maximum near the center. This non-uniform force reduces the axial flow velocity of the central stream of the pipe. To keep the mass flow uniform the fluid has to flow adjacent to the pipe wall and hence the dimensionless axial velocity near the pipe wall increases. Further, from these figures one can notice that the velocity profile becomes flatter with an increase in the Hartmann number.

Figs. 6–8 show the effects of R, $\boldsymbol{\alpha}$, and M on the dimensionless radial velocity. Fig. 6a and b demonstrate the effect of permeation Reynolds number R on the dimensionless radial velocity for $\boldsymbol{\alpha} = 2$ and $\boldsymbol{\alpha} = -2$. For constant $\boldsymbol{\alpha}$, the absolute dimensionless radial velocity increases with increasing suction while it decreases with increasing injection. The effect of wall expansion ratio $\boldsymbol{\alpha}$ on the dimensionless radial velocity is shown

Please cite this article in press as: Srinivas S et al., Influence of heat transfer on MHD flow in a pipe with expanding or contracting permeable wall, Ain Shams Eng J (2014), http://dx.doi.org/10.1016/j.asej.2014.01.006

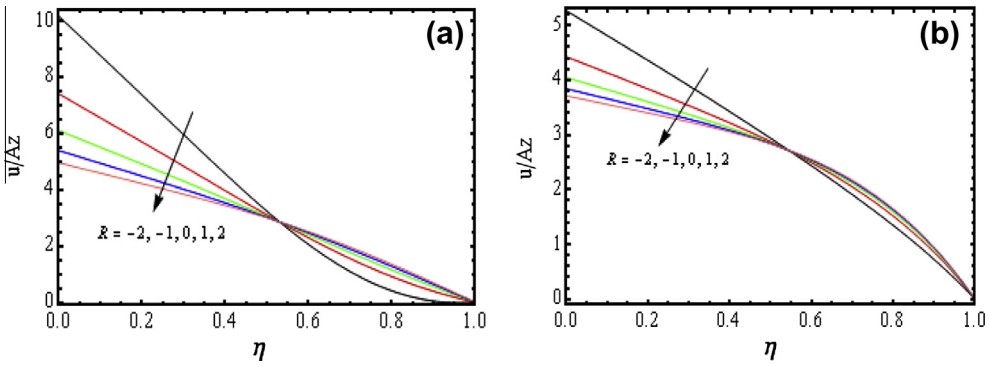

Figure 3 Axial velocity over a range of R. (a) $\alpha = 2$, $M = 1$, (b) $\alpha = -2$, $M = 1$.

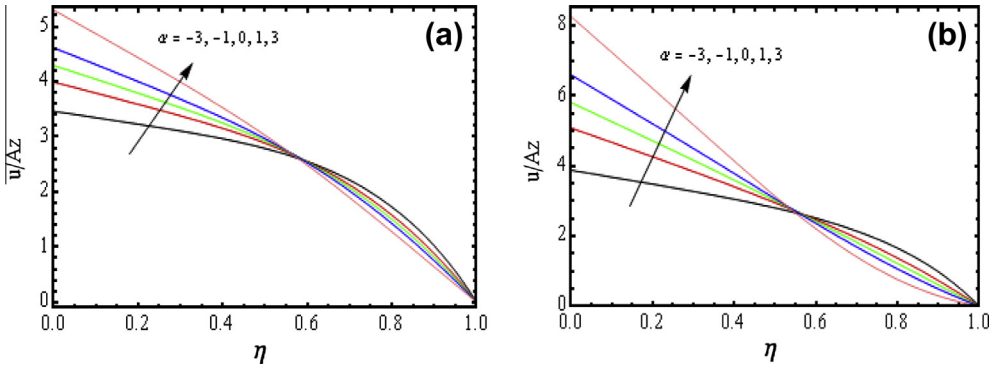

Figure 4 Axial velocity over a range of α. (a) $R = 2$, $M = 1$, (b)$R = -1$, $M = 1$.

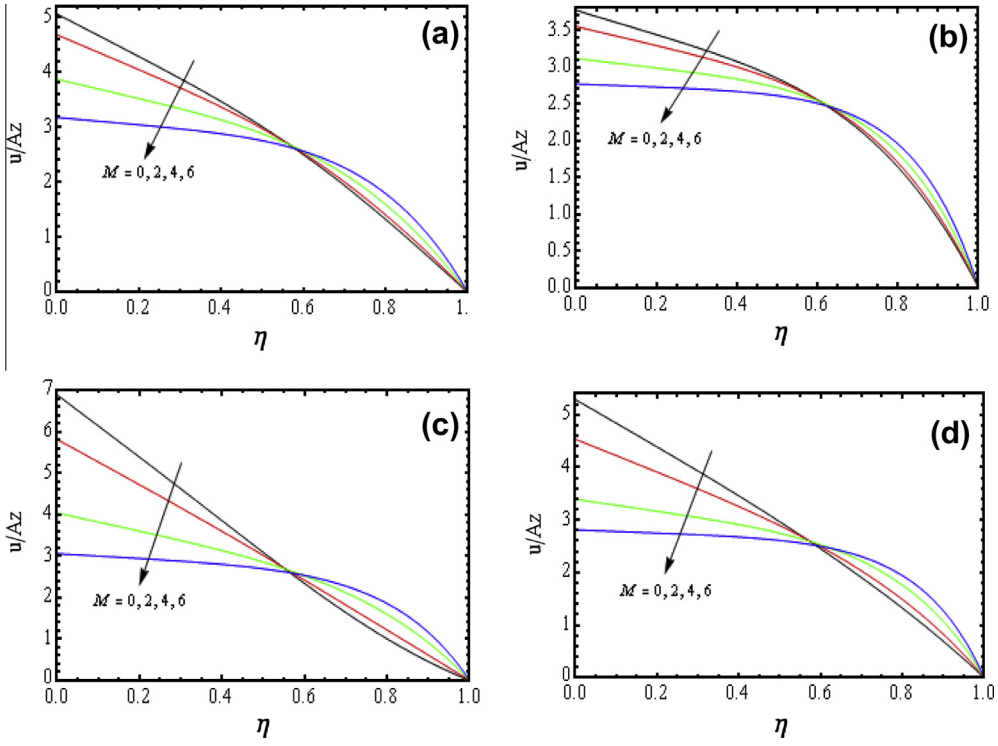

Figure 5 Axial velocities for different M. (a) $R = 2$, $\alpha = 2$, (b) $R = 2$, $\alpha = -2$, (c) $R = -1$, $\alpha = 1$, (d) $R = -1$, $\alpha = -1$.

Please cite this article in press as: Srinivas S et al., Influence of heat transfer on MHD flow in a pipe with expanding or contracting permeable wall, Ain Shams Eng J (2014), http://dx.doi.org/10.1016/j.asej.2014.01.006

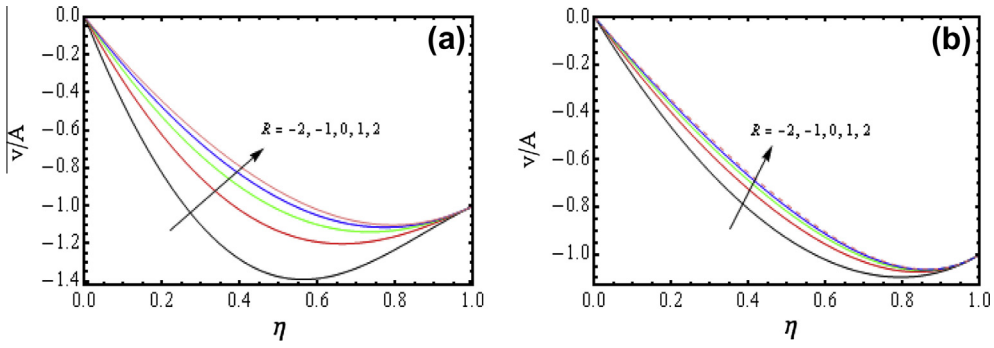

Figure 6 Radial velocity over a range of R. (a) $\alpha = 2$, $M = 1$, (b) $\alpha = -2$, $M = 1$.

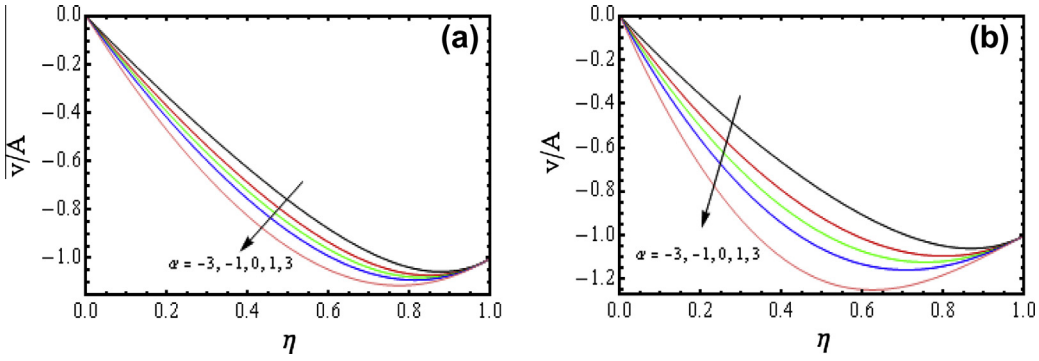

Figure 7 Radial velocity over a range of α. (a) $R = 2$, $M = 0.5$, (b) $R = -1$, $M = 0.5$.

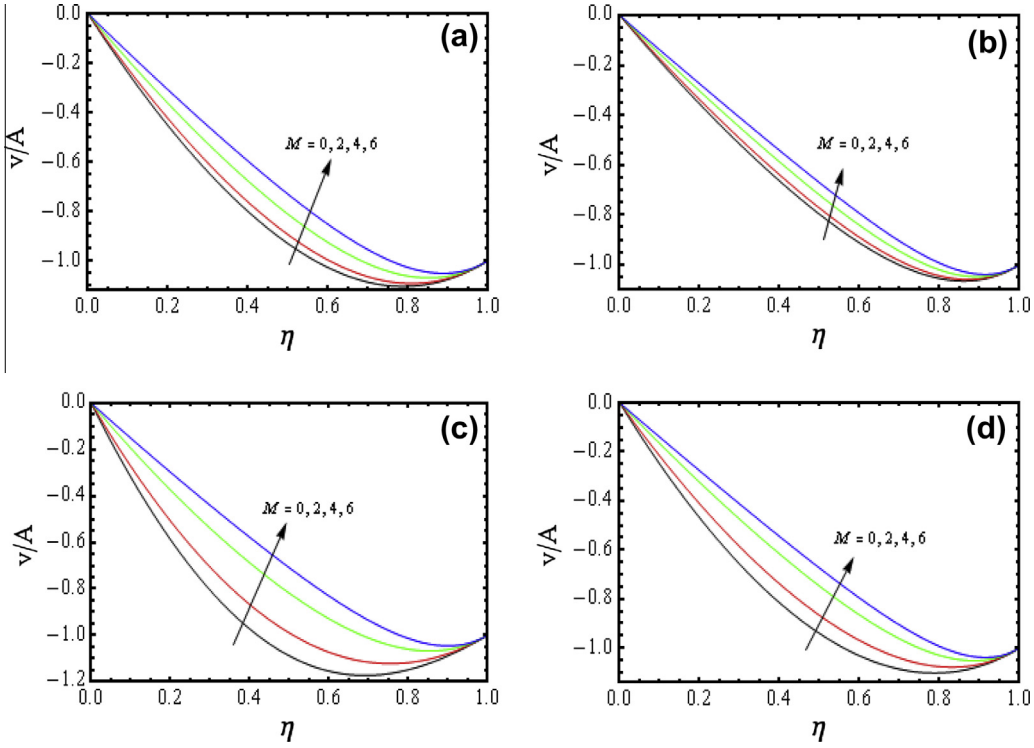

Figure 8 Radial velocity for different M. (a) $R = 2$, $\alpha = 2$, (b) $R = 2$, $\alpha = -2$, (c) $R = -1$, $\alpha = 1$, (d) $R = -1$, $\alpha = -1$.

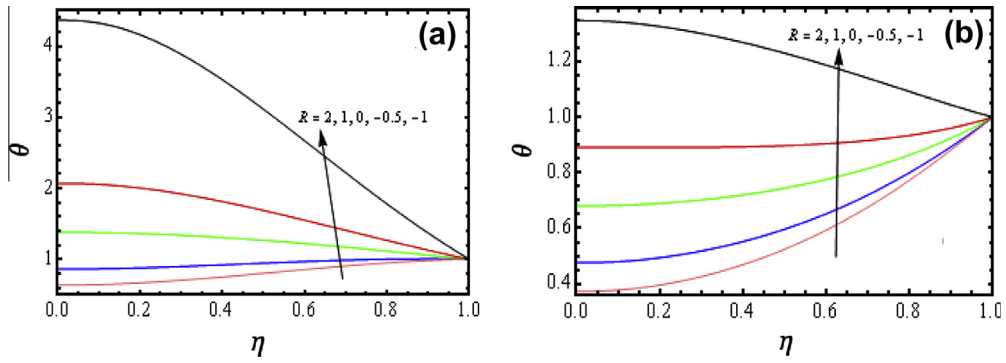

Figure 9 Effect of R on temperature distribution. (a) $\alpha = 2$, $M = 1$, Pr = 0.71, (b) $\alpha = -2$, $M = 1$, Pr = 0.71.

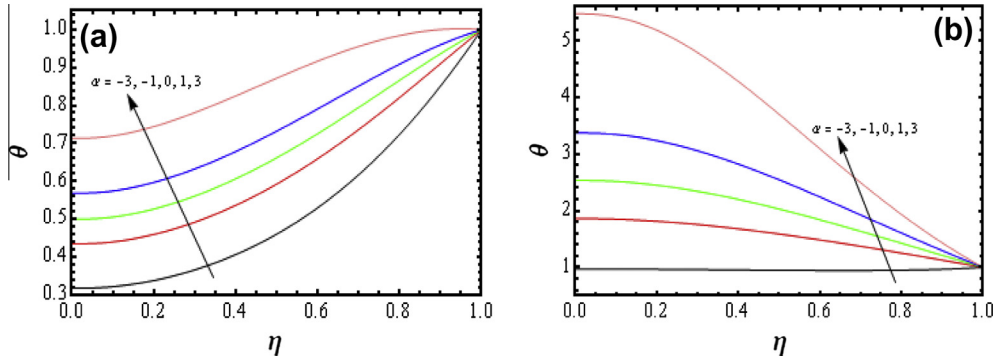

Figure 10 Effect of α on temperature distribution. (a) $R = 2$, $M = 1$, Pr = 0.71, (b) $R = -1$, $M = 1$, Pr = 0.71.

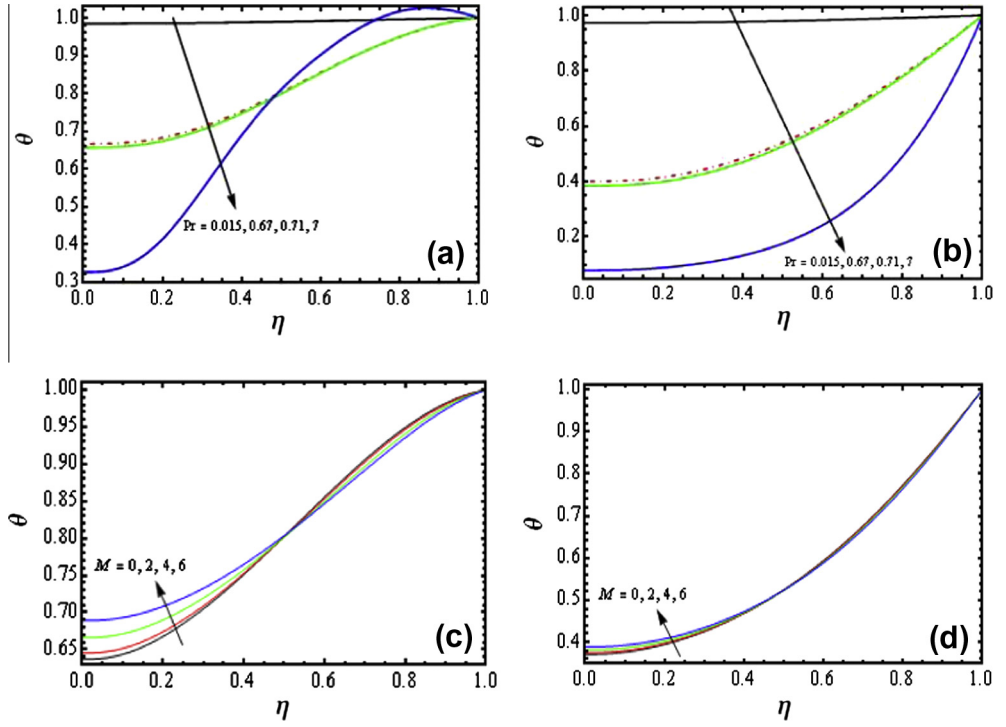

Figure 11 Temperature distribution. (a) $R = 2$, $M = 1$, $\alpha = 2$, (b) $R = 2$, $M = 1$, $\alpha = -2$, (c) $R = 2$, Pr = 0.71, $\alpha = 2$, (d) $R = 2$, Pr = 0.71, $\alpha = -2$.

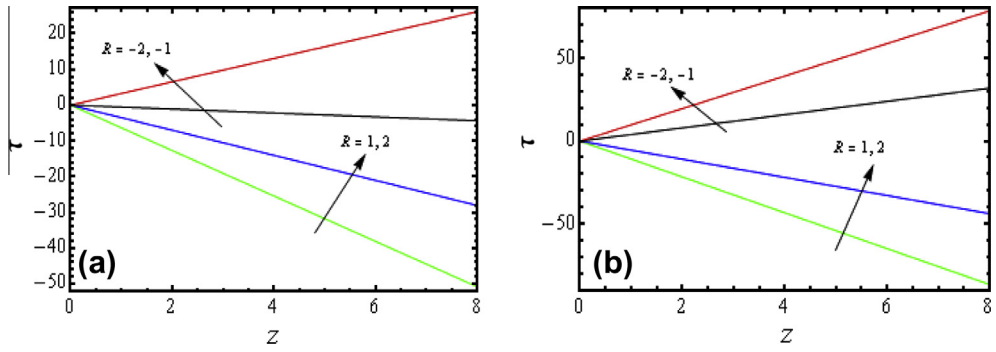

Figure 12 Effect of R on wall shear stress distribution. (a) $\alpha = 2$, $M = 1$ (b) $\alpha = -2$, $M = 1$.

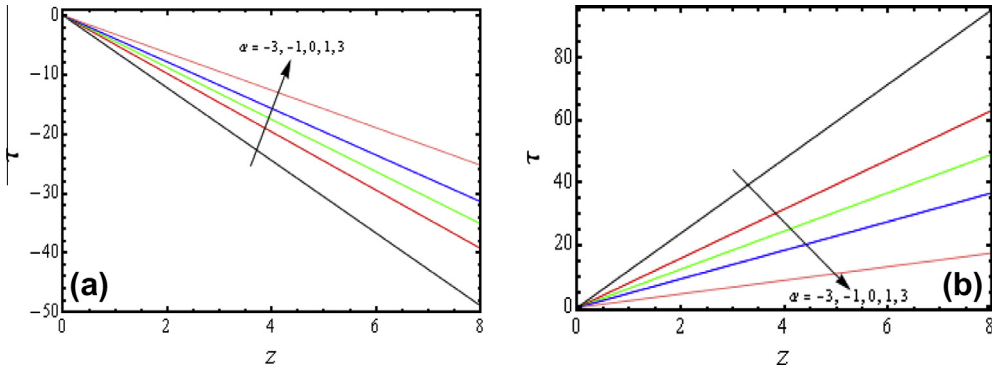

Figure 13 Effect of α on wall shear stress distribution. (a) $R = 2$, $M = 1$, (b) $R = -1$, $M = 1$.

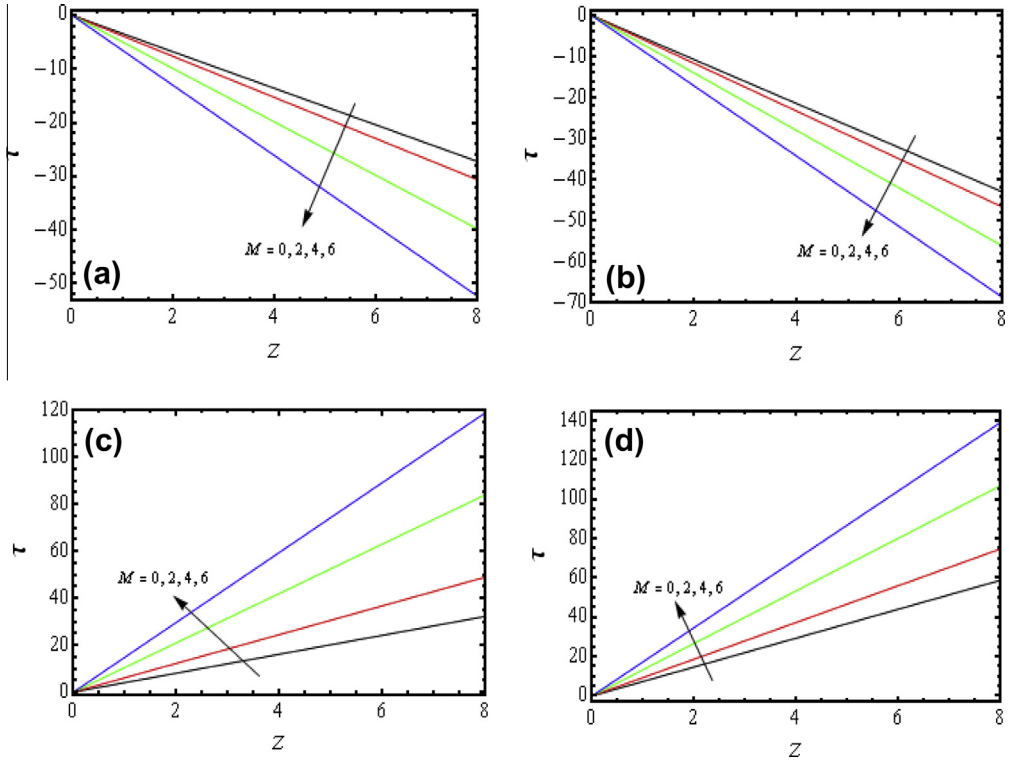

Figure 14 Wall shear stress distribution for different M. (a) $R = 2$, $\alpha = 2$, (b) $R = 2$, $\alpha = -2$ (c) $R = -1$, $\alpha = 1$, (d) $R = -1$, $\alpha = -1$.

Please cite this article in press as: Srinivas S et al., Influence of heat transfer on MHD flow in a pipe with expanding or contracting permeable wall, Ain Shams Eng J (2014), http://dx.doi.org/10.1016/j.asej.2014.01.006

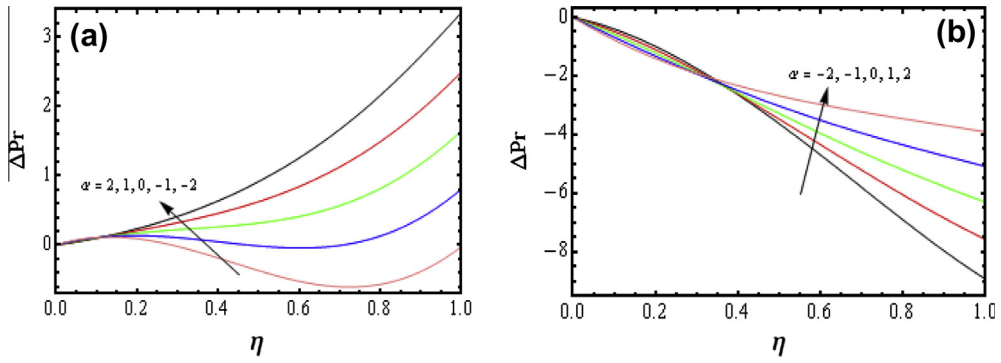

Figure 15 Radial pressure drop over a range of α. (a) $R = 2$, $M = 1$, (b)$R = -1$, $M = 1$.

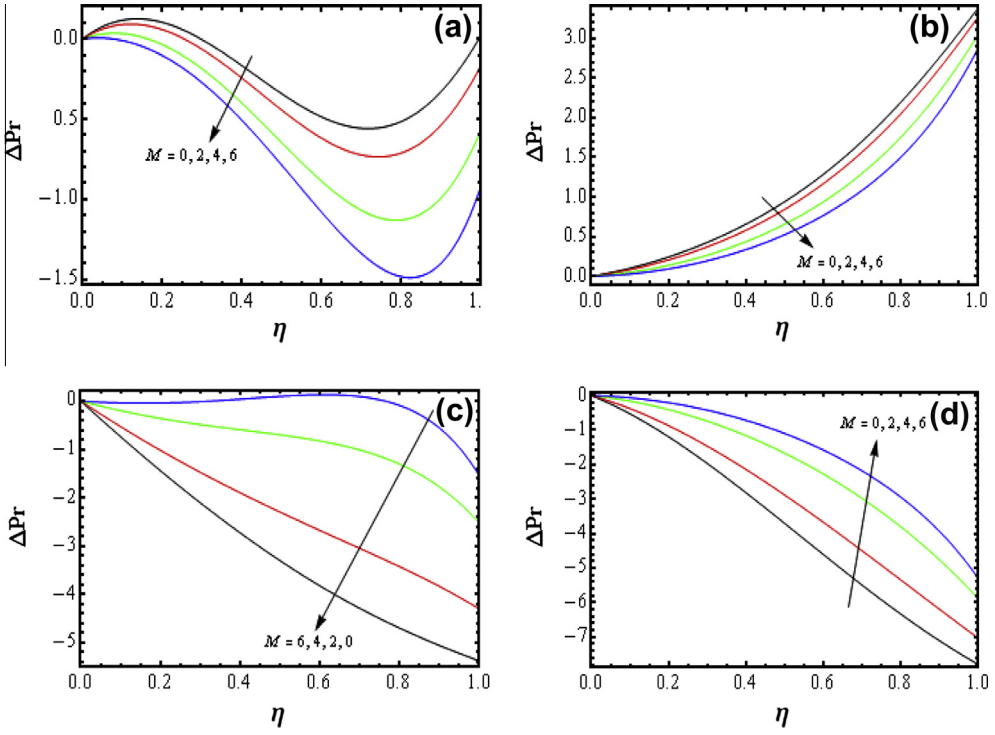

Figure 16 Radial pressure drop for different M. (a) $R = 2$, $\alpha = 2$, (b) $R = 2$, $\alpha = -2$, (c) $R = -1$, $\alpha = 1$, (d) $R = -1$, $\alpha = -1$.

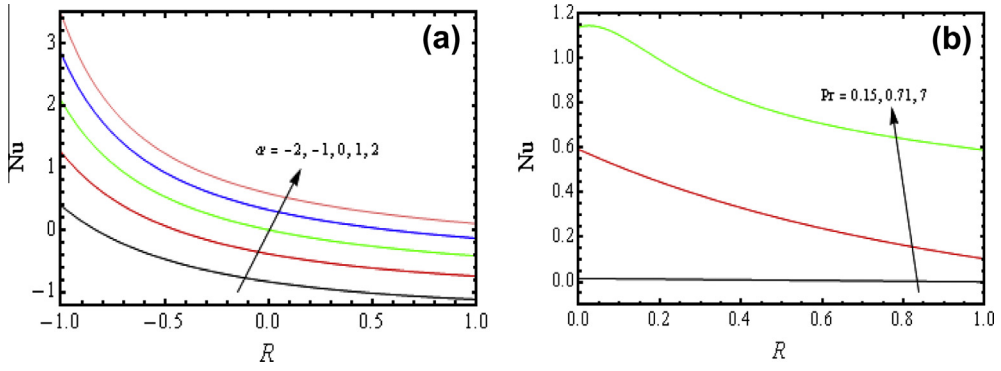

Figure 17 Nusselt number distribution. (a) Effect of α when $M = 0.5$, Pr = 1, (b) effect of Pr when $\alpha = 2$, $M = 0.5$.

Table 2 Radial velocity observations in case of suction for different values of α.

α	η	v/A	v/A	v/A
		Boutros et al. (Ref. [11])	HAM(15th order)	HAM(20th order)
(a) M = 0, R = −100				
50	0.91652	−1.039776	−1.03942	−1.03641
20	0.88318	−1.053519	−1.05628	−1.05519
0	0.86023	−1.067444	−1.06864	−1.06842
−5	0.86023	−1.071578	−1.07157	−1.07151
−10	0.84853	−1.076252	−1.07491	−1.07492
(b) M = 0, R = −1000				
50	0.87178	−1.062978	−1.06573	−1.06527
20	0.86023	−1.065272	−1.06781	−1.06736
0	0.86023	−1.066926	−1.06897	−1.06859
−5	0.86023	−1.067339	−1.06926	−1.06889
−10	0.86023	−1.067752	−1.06954	−1.06919

in Fig. 7a and b. For every level of injection or suction, for the case of wall contraction, the absolute dimensionless radial velocity decreases as increasing $|\alpha|$ whereas it increases as α increases for the case of wall expansion. Fig. 8a–d shows the influence of Hartmann number on the dimensionless radial velocity. From these figures one can observe that the absolute dimensionless radial velocity decreases as Hartmann number increases. The reason of this is the magnetic field is normal to the flow and has the tendency to slow down the radial movement of the fluid in pipe because it gives rise to a resistive force namely the Lorentz force which acts opposite to the flow and radial directions.

Figs. 9–11 illustrate the effects of R, α and Pr on dimensionless temperature distribution θ. Fig. 9a and b shows the effect of permeation Reynolds number R on the dimensionless temperature distribution. For a given increase in injection the boundary layer thickness decreases and as a result θ decreases for both the cases of injection combined with wall expansion and contraction. The behavior is reversed for suction combined with wall expansion and contraction. Fig. 10a and b demonstrates the effect of wall expansion ratio α on θ. For every level of suction or injection, θ increases as α increases for the case of wall expansion while it decreases as $|\alpha|$ increases for the case of wall contraction. Fig. 11a and b depict the effect of Prandtl number Pr (i.e. Pr = 0.015, 0.67, 0.71, 7 for mercury, Argon at 25^0c, air and water respectively) on θ. As anticipated with increasing Prandtl number Pr (i.e. with decreasing thermal diffusivity), the thermal boundary layer thickness decreases. So the dimensionless temperature decreases. From Fig. 11c and d it is clear that near the center θ increases for a given increase in the Hartmann number M and decreases apart from the center for both the cases wall expansion and contraction combined with injection.

The effects of R, α, and M on the dimensionless wall shear stress are shown in Figs. 12–14. The absolute wall shear stress increases along the wall surface in proportion to z. Fig. 12a and b shows that for constant wall expansion ratio α the absolute wall shear stress decreases as increasing R while it increases as $|R|$ increases. The effect of wall expansion ratio on dimensionless wall shear stress is shown in Fig. 13a and b. For every level of injection or suction, for the case of wall expansion the absolute wall shear stress decreases as α increases while it increases as $|\alpha|$ increases for the case of wall contraction. Fig. 14a–d illustrates the effect of Hartmann number M on dimensionless wall shear stress. From these figures one can observe that the absolute wall shear stress increases as M increases which may be due to an increase in velocity gradient at the pipe wall (see Fig. 5).

Figs. 15 and 16 illustrate the effects of α and M on the dimensionless radial pressure distribution. Fig. 15a and b shows the effect of wall expansion ratio α on the dimensionless radial pressure distribution. For every level of injection or suction, the absolute radial pressure distribution $|\Delta P_r|$is lower near the central portion. For the case of wall expansion, increasing α leads to lower $|\Delta P_r|$ and for the case of wall contraction increasing $|\alpha|$ leads to higher $|\Delta P_r|$. Fig. 16a–d shows the effect of Hartmann number M on the dimensionless radial pressure distribution. From these figures one can see that $|\Delta P_r|$ decreases as M increases.

Fig. 17 indicates the variation in Nusselt number distribution Nu for different values of α and Pr against R. Fig. 17a depicts for the case of wall expansion, Nu increases with the increase of α, while it decreases as $|\alpha|$ increases at the pipe wall $\eta = 1$. Fig. 17b shows that Nu increases as Pr increase at the wall $\eta = 1$, which is due to the progressive thinning of the thermal boundary layer.

The radial velocity observations for different values of α, for the case of hydrodynamic viscous flow in a semi-infinite expanding or contracting porous pipe have been shown in Table 2. Tables 2(a) and (b) correspond to the case of suction i.e. for $R = -100$, $R = -1000$ respectively. The numerical values presented in these Tables are in good agreement with the results reported by Botrous et al. [11].

4. Conclusions

This investigation deals with the analysis of heat transfer and MHD viscous flow in a porous pipe with expanding or contracting wall. Using suitable similarity transformations, the governing equations are reduced to a system of coupled nonlinear differential equations. The resulting equations are solved by employing the homotopy analysis method (HAM). The influence of pertinent parameters (such as the permeation Reynolds number, wall expansion ratio, and Hartmann number) on dimensionless velocity components, temperature, wall shear stress, radial pressure drop and Nusslet number distributions has been discussed through graphs. The results show that they have a strong influence on the flow variables. The main findings are summarized as follows:

Please cite this article in press as: Srinivas S et al., Influence of heat transfer on MHD flow in a pipe with expanding or contracting permeable wall, Ain Shams Eng J (2014), http://dx.doi.org/10.1016/j.asej.2014.01.006

- For a constant wall expansion ratio α, the dimensionless axial velocity near the center increases with increasing suction while decreases with increasing injection.
- For given increase in M, the dimensionless axial velocity decreases little away the pipe wall. For every level of injection or suction, for the case of wall contraction, the absolute dimensionless radial velocity decreases with increasing $|\alpha|$ whereas it increases as α increases for the case of wall expansion. The absolute dimensionless radial velocity decreases as M increases.
- For every level of suction or injection, θ increases as α increases for the case of wall expansion while it decreases as $|\alpha|$ increases for the case of wall contraction. Further, θ decreases with increasing Pr .
- The absolute wall shear stress increases as M increases.
- The absolute axial pressure distribution $|\Delta P_r|$ decreases as M increases.
- The problem related to the porous pipe flow with stationary wall can be recovered from our analysis in the limiting case of $\alpha = 0$.

Acknowledgment

One of the authors (S.S.) gratefully acknowledges DST, Government of India for sanctioning a major research project under the Grant Number SR/SL.MS: 674/10.

References

[1] Majdalani J, Zhou C, Dawson CA. Two-dimensional viscous flow between slowly expanding or contracting walls with weak permeability. J Biomech 2002;35:1399–403.
[2] Berman AS. Laminar flow in channel with porous walls. J Appl Phys 1953;24:1232–5.
[3] Weissberg HL. Laminar flow in the entrance region of a porous pipe. Phys Fluids 1959;2:510–6.
[4] Terrill RM, Thomas PW. Laminar flow in a uniformly porous pipe. Appl Sci Res 1969;21:37–67.
[5] Terrill RM, Thomas PW. Spiral flow in a porous pipe. Phys Fluids 1973;16:356–9.
[6] Cox SM. Two dimensional flow of a viscous fluid in a channel with porous walls. J Fluid Mech 1991;227:1–33.
[7] Majdalani J, Flandro GL. The oscillatory pipe flow with arbitrary injection. Proc Roy Soc Lond A 2002;458:1621–51.
[8] Uchida S, Aoki H. Unsteady flows in a semi-infinite contracting or expanding pipe. J Fluid Mech 1977;82:371–81.
[9] Goto M, Uchida S. Unsteady flows in a semi-infinite contracting or expanding pipe with a porous wall. Theor Appl Mech 1991;40:161–72.
[10] Bujurke NM, Pai NP, Jayaraman G. Computer extended series solution for unsteady flow in a contracting or expanding pipe. IMA J Appl Math 1998;60:151–65.
[11] Boutros YZ, Abd-el-Malek MB, Bdran NA, Hassan HS. Lie-group method for unsteady flows in a semi-infinite expanding or contracting pipe with injection or suction through a porous wall. J Comput Appl Math 2006;197:465–94.
[12] Xinhui S, Liancun Z, Xinxin Z, Jainhong Y, Ying C. Multiple solutions for the laminar flow in a porous pipe with suction at slowly expanding or contracting wall. Appl Math Comput 2011;218:3515–21.
[13] Majdalani J, Zhou C. Moderate-to-large injection and suction driven channel flows with expanding or contracting walls. Z Angew Math Mech 2003;83:181–96.
[14] Hayat T, Iqbal Z, Sajid M, Vajravelu K. Heat transfer pipe flow of a Johnson–Segalman fluid. Int Comm Heat Mass Transfer 2008;35:1297–307.
[15] Muthuraj R, Srinivas S. A note on heat transfer MHD oscillatory flow in an asymmetric wavy channel. Int Commun Heat Mass Transfer 2010;37:1255–60.
[16] Mukhopadhyay S. MHD boundary layer slip flow along a stretching cylinder. Ain Shams Eng J 2013;4:317–24.
[17] Malekzadeh A, Heyderinasab A, Dabir B. Magnetic field effect on fluid flow characteristics in a pipe for laminar flow. J Mech Sci Technol 2011;25:333–9.
[18] Sweet E, Vajravelu K, Gorder RAV, Pop I. Analytical solutions for the unsteady MHD flow of a viscous fluid between parallel plates. Commun Nonlinear Sci Numer Simulat 2011;16:266–73.
[19] Hayat T, Sajid M, Ayub M. On explicit analytic solution for MHD pipe flow of fourth grade fluid. Commun Nonlinear Sci Numer Simulat 2008;13:745–51.
[20] Si X, Zheng L, Zhang X, Chao Y. Perturbation solution to unsteady flow in a porous channel with expanding or contracting walls of a transverse magnetic field. Appl Math Mech-Engl Ed 2010;31:151–8.
[21] Turkyilmazoglu M. Exact solutions corresponding to the viscous incompressible and conducting fluid flow due to a rotating disk. Z Angew Math Mech 2009;89:490–503.
[22] Makinde OD, Aregbesola YAS, Odejide SA. Wall driven steady flow and heat transfer in a porous tube. Kragujevac J Math 2006;29:193–201.
[23] Nakhi AB, Chamkha AJ. Conjugate natural convection around a finned pipe in a square enclosure with internal heat generation. Int J Heat Mass Transfer 2007;50:2260–71.
[24] Srinivas S, Subramanyam Reddy A, Ramamohan TR. A study on thermal-diffusion and diffusion-thermo effects in a two-dimensional viscous flow between slowly expanding or contracting walls with weak permeability. Int J Heat Mass Transfer 2012;55:3008–20.
[25] Subramanyam Reddy A, Srinivas S, Ramamohan TR. Analysis of heat and chemical reaction on an asymmetric laminar flow between slowly expanding or contracting walls. Heat Transfer-Asian Res 2013;42:422–43.
[26] Srinivas S, Subramanyam Reddy A, Ramamohan TR. Mass transfer effects on viscous flow in an expanding or contracting porous pipe with chemical reaction. Heat Transfer-Asian Research; 2014 (in press).
[27] Liao SJ. Beyond perturbation: introduction to homotopy analysis method. Boca Raton: CRC Press, Chapman and Hall; 2003.
[28] Hang X, Lin ZL, Liao SJ, Majdalani J. Homotopy based solutions of the Navier–Stokes equations for a porous channel with orthogonally moving walls. Phys Fluids 2010;22:053601–53618.
[29] Hang X, Liao SJ, Pop I. Series solution of unsteady boundary layer flows of non-Newtonian fluids near a forward stagnation point. J Non-Newtonian Fluid Mech 2006;139:31–43.
[30] Abbasbandy S. The application of homotopy analysis method to nonlinear equations arising heat transfer. Phys Lett A 2006;360:109–13.
[31] Si X, Zheng L, Zhang X, Chao Y. Homotopy analysis solution for the asymmetric laminar flow in a porous channel with expanding or contracting walls. Acta Mech Sin 2011;27:208–14.
[32] Sajid M, Abbas Z, Hayat T. Homotopy analysis for boundary layer flow of micropolar fluid through porous channel. Appl Math Model 2009;33:4120–5.
[33] Xu H, Pop I. Homotopy analysis of unsteady-boundary layer flow saturated impulsively from rest along a symmetric wedge. Z Angew Math Mech 2008;88:507–14.
[34] Turkyilmazoglu M. Purely analytic solutions of Magnetohydrodynamic swirling boundary layer flow over a rotating porous disk. Comput Fluids 2010;39:793–9.
[35] Srinivas S, Gupta A, Gulati S, Subramanyam Reddy A. Flow and mass transfer effects on viscous fluid in a porous channel with moving/stationary walls in presence of chemical reaction. Int Commun Heat Mass Transfer 2013;48:34–9.

S. Srinivas obtained his Doctoral Degree from NIT(formerly REC), Warangal, India. He has about 27 years of teaching and research experience. He has research interests in MHD flows, Heat and Mass Transfer, Boundary layer flows, Non-Newtonian flows, Nanofluids He has published 72 research papers in various journals and conference proceedings. The total citations of his papers, as per Google Scholar, exceeds 1000. He is a reviewer for several international journals. Presently he is a Senior Professor in the Fluid Dynamics Division of School of Advanced Sciences at VIT University, Vellore, India.

A. Subramanyam Reddy is a Senior Research Fellow (Department of Science and Technology Govt. of India) in the department of Mathematics VIT University, Vellore, India. He obtained Maters degree in Mathematics from the Sri Venkateswara University, Trupati, India. He is pursuing Ph.D. in the field of Fluid Dynamics at VIT University Vellore. He has teaching experience of 7 years and research experience of 3 years. He has published 5 research papers in refereed journals.

T.R. Ramamohan is a Chief-Scientist at the *CSIR* Centre for Mathematical Modelling and Computer Simulation (C-MMACS), Bangalore, India. He received his B.Tech (Chemical Engineering) degree from IIT Chennai and obtained his M.S & Ph.D. Degrees from Northwestern University, USA. He has given several invited lectures at colleges and universities throughout the country. Dr. Ramamohans's extensive experience in Mathematical modeling is evidenced by (nearly) 80 publications in international journals of high repute in addition to another 20 papers in conference proceedings. Further, he has one patent to his credit. His current research interests are fluid dynamics and nonlinear dynamics.

Anant Kant Shukla is a Senior Research Fellow (CSIR) at CSIR Centre for Mathematical Modelling and Computer Simulation, Council of Scientific and Industrial Research Bangalore, India. He obtained Maters degree in Mathematics from C.S.J.M University (formerly Kanpur University), Kanpur, India. His current interests are Nonlinear dynamics and fluid dynamics. He has published 3 research papers in refereed journals.

Please cite this article in press as: Srinivas S et al., Influence of heat transfer on MHD flow in a pipe with expanding or contracting permeable wall, Ain Shams Eng J (2014), http://dx.doi.org/10.1016/j.asej.2014.01.006